ADVANCED MATERIALS
www.advmat.de

Mixing Insulating Commodity Polymers with Semiconducting n-type Polymers Enables High-Performance Electrochemical Transistors

Erica Zeglio, Yazhou Wang, Saumey Jain, Yunfan Lin, Alan Eduardo Avila Ramirez, Kui Feng, Xugang Guo, Helena Ose, Gatis Mozolevskis, Damia Mawad, Wan Yue, Mahiar Max Hamedi, and Anna Herland**

Diluting organic semiconductors with a host insulating polymer is used to increase the electronic mobility in organic electronic devices, such as thin film transistors, while considerably reducing material costs. In contrast to organic electronics, bioelectronic devices such as the organic electrochemical transistor (OECT) rely on both electronic and ionic mobility for efficient operation, making it challenging to integrate hydrophobic polymers as the predominant blend component. This work shows that diluting the n-type conjugated polymer p(N-T) with high molecular weight polystyrene (10 KDa) leads to OECTs with over three times better mobility-volumetric capacitance product (μC*) with respect to the pristine p(N-T) (from 4.3 to 13.4 F V^{-1} cm^{-1} s^{-1}) while drastically decreasing the amount of conjugated polymer (six times less). This improvement in μC* is due to a dramatic increase in electronic mobility by two orders of magnitude, from 0.059 to 1.3 cm^2 V^{-1} s^{-1} for p(N-T):Polystyrene 10 KDa 1:6. Moreover, devices made with this polymer blend show better stability, retaining 77% of the initial drain current after 60 minutes operation in contrast to 12% for pristine p(N-T). These results open a new generation of low-cost organic mixed ionic-electronic conductors where the bulk of the film is made by a commodity polymer.

1. Introduction

Organic mixed ionic-electronic conductors are materials that exhibit mixed electronic and ionic conductivity, allowing a wide range of applications, from actuation and sensing to energy conversion and storage.[1,2] Their low operating voltages, tunable properties, and ease of processing enabled their use in bioelectronic devices such as stimulating electrodes, ion pumps, neuromorphic circuits, and organic electrochemical transistors (OECTs).[3] The OECT is a transducing amplifier that uses a mixed ionic-electronic conductor in the form of a thin film between source and drain contacts, through which electronic charge carriers are transported.[4,5] The concentration of such charge carriers is modulated by the penetration or extraction of electrolyte ions upon application of a gate bias. For most applications, the electrolyte is water-based, meaning that the

E. Zeglio, A. Herland
AIMES-Center for the Advancement of Integrated Medical and Engineering Sciences
Department of Neuroscience
Karolinska Institute
Solna 171 77, Sweden
E-mail: erica.zeglio@mmk.su.se; aherland@kth.se

E. Zeglio, S. Jain, Y. Lin, A. E. Avila Ramirez, A. Herland
Division of Nanobiotechnology
Department of Protein Science
Science for Life Laboratory
School of Engineering Sciences in Chemistry
Biotechnology and Health
KTH Royal Institute of Technology
Solna 171 65, Sweden

The ORCID identification number(s) for the author(s) of this article can be found under https://doi.org/10.1002/adma.202302624

DOI: 10.1002/adma.202302624

E. Zeglio, W. Yue
Wallenberg Initiative Materials Science for Sustainability
Department of Materials and Environmental Chemistry
Stockholm University
Stockholm 114 18, Sweden

E. Zeglio, M. M. Hamedi
Digital Futures
Stockholm SE-100 44, Sweden

Y. Wang
State Key Laboratory of Optoelectronic Materials and Technologies
Key Laboratory for Polymeric Composite and Functional Materials of Ministry of Education
Guangzhou Key Laboratory of Flexible Electronic Materials and Wearable Devices
School of Materials Science and Engineering
Sun Yat-sen University
Guangzhou 510275, P. R. China

thin film must adjust to the inclusion of hydrated electrolyte ions throughout the bulk of the material upon device switching.

π-conjugated polymers are the most common type of mixed ionic-electronic conductors used as core OECT components.[4,6] They can be classified as p- or n-type depending on their ability to stabilize holes or electrons as charge carriers, respectively. While both types of materials are important for several bioelectronic applications, such as biosensors and complementary circuits, n-type conjugated polymers had a relatively slower development with respect to their p-type counterpart.[7] Molecular design strategies have thereby been adopted to ensure that also n-type conjugated polymers provide a good balance of ionic and electronic mobility and stability in OECT device operation. Examples include introducing new building blocks,[8] functional groups,[9] and balancing the number, position, and extent of side groups, such as glycol and alkyl side chains.[10,11] Other strategies, besides chemical structure modifications, include solvent engineering, incorporating additives, or blending with other materials to enhance the overall performance of the OECT device.[12–14]

Most efforts on polymer blends for OECTs are restricted to charged or hydrophilic polymers used as dopants or to provide new functionalities. Blending with charged polymer dopants led to some of the most remarkable examples of conducting polymer blends. Poly(3,4-ethylene-dioxythiophene) doped with poly(styrene sulfonate) PEDOT:PSS is one of the most investigated p-type organic conductor, providing hole conductivity over 1000 S cm^{-1} and excellent ambient stability.[15] Similarly, a recent example of an n-type mixed ionic-electronic conductor is poly(benzimidazobenzophenanthroline):poly(ethyleneimine) (BBL:PEI), leading to conductivity up to 7.7 ± 0.5 S cm^{-1} for 50 wt% PEI content.[12] Blending with polar insulating polymers introduced new functionalities, such as hydroxyl groups for biofunctionalization or radical groups for doping.[16,17] An example is the ternary blend of PEDOT:PSS with polyvinylalcohol (PVA).[17] However, for this blend, incorporation of the PVA component led to a decrease in film conductivity and a subsequent degradation in OECT performance.

Polymer blends formed by "diluting" organic semiconductors with a "host" insulating polymer have been introduced to improve electronic performance, stability, and processability in optoelectronic devices, including organic light-emitting diodes (OLEDs), solar cells, and field-effect transistors (FETs).[18–22] The most remarkable result of integrating high concentrations of insulators into organic semiconducting films, leading to the so-called "diluted organic semiconductors," is the dramatic decrease in charge trapping, leading to an enhancement in charge carrier mobility by several orders of magnitude.[18] For example, blending poly(3-hexylthiophene) P3HT with polystyrene (PS) resulted in FETs where the concentration of the semiconductor was reduced to values as low as 3 wt%.[23] Such a strategy provides the double advantage of improving device performance while abating material costs, considering that insulating polymers such as PS and polyvinyl carbazole (PVK) are commodity materials synthesized at a fraction of the cost compared to most organic semiconductors.[18]

Despite these benefits, to date, there has been no attempt to blend organic mixed ionic-electronic conductors with large amounts of insulating polymers to increase the performance of OECTs. The main challenge is that the high-bandgap polymers that have been tested so far as host materials, such as PS, PVK, and poly(9,9-di-n-octylfluorenyl-2,7-diyl) (PFO), are very hydrophobic. While hydrophobicity is not an issue for organic electronic devices that rely only on electronic transport, such as FETs, the impact of the host polymer on the mixed ionic-electronic conductivity of the films and OECT operation is not straightforward.

In this work, we show that dilution of the n-type semiconductor p(N-T), a copolymer based on aza-substituted bis(2-oxoindolin-3-ylidene)-benzodifuran-dione acceptor units and thiophene donor units (see **Figure 1a** for chemical structure), with PS drastically increases the electronic mobility and provides iontronic conductivity in water. We demonstrate that this new generation of OECT materials, made using the diluted semiconductor strategy, show better device performance and stability with respect to pristine conjugated polymer-only OECTs. In addition, we elucidate the impact of the hydrophilicity and molecular weight of the insulator component on the mixed ionic/electronic conductivity of the films.

2. Results and Discussion

We chose p(N-T) polymer because of its good processability, allowing the preparation of bicomponent blends from organic solvents such as chloroform and o-dichlorobenzene. OECTs made using p(N-T) exhibit a low threshold voltage of 0.25 V and normalized transconductance of 0.72 S cm^{-1} deriving from p(N-T) mixed ionic/electronic conductivity, with an average product of mobility and volumetric capacitance μC* of 4.3 F cm^{-1} V^{-1} s^{-1}.[24]

S. Jain
Division of Micro and Nanosystems
Department of Intelligent Systems
School of Electrical Engineering and Computer Science
KTH Royal Institute of Technology
Stockholm 100 44, Sweden

K. Feng
Academy for Advanced Interdisciplinary Studies
Southern University of Science and Technology (SUSTech)
Shenzhen, Guangdong 518055, China

K. Feng, X. Guo
Department of Materials Science and Engineering
Southern University of Science and Technology (SUSTech)
Shenzhen, Guangdong 518055, China

X. Guo
Guangdong Provincial Key Laboratory of Functional Oxide Materials and Devices
Southern University of Science and Technology (SUSTech)
Shenzhen, Guangdong 518055, China

H. Ose, G. Mozolevskis
Micro and nanodevices laboratory
Institute of Solid-State Physics
University of Latvia
8 Kengaraga Str., Riga LV-1063, Latvia

D. Mawad
School of Materials Science and Engineering
UNSW Sydney
Sydney, New South Wales 2052, Australia

M. M. Hamedi
Department of Fiber and Polymer Technology
School of Engineering Sciences in Chemistry, Biotechnology and Health
KTH Royal Institute of Technology
Teknikringen 56, Stockholm 100 44, Sweden

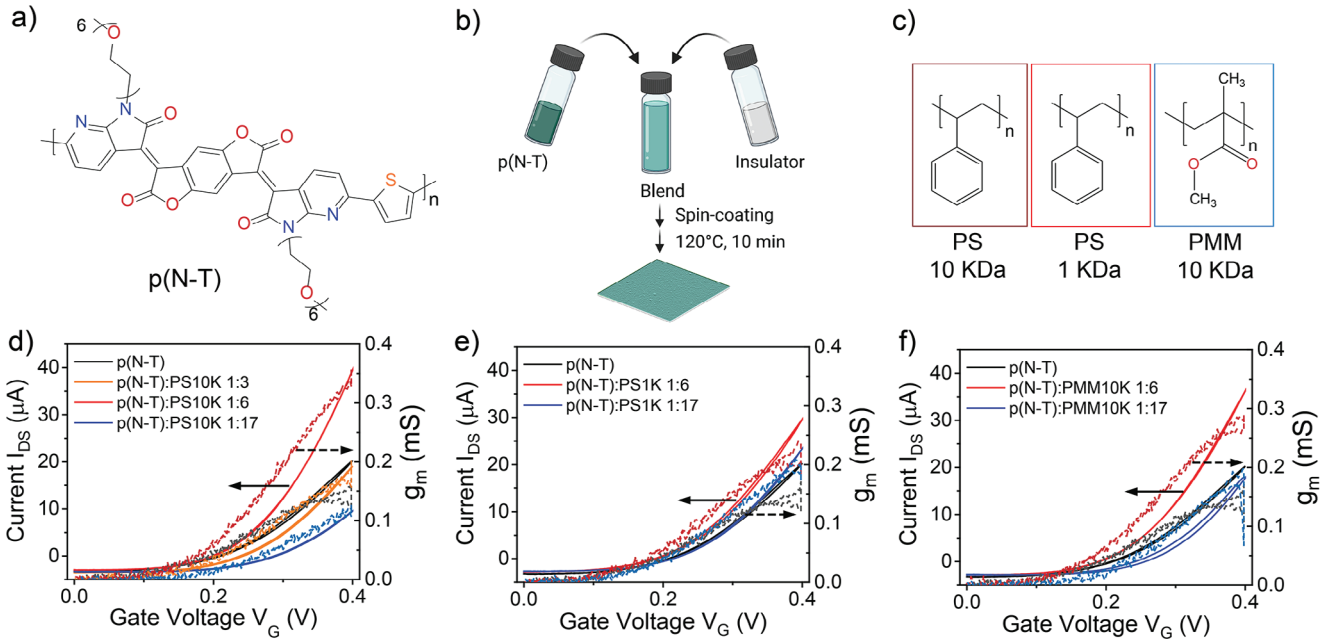

Figure 1. a) Chemical structure of p(N-T). b) Illustration of the process of blending and preparation of thin films of the blend. c) Chemical structure of the insulating polymers used in this study. Transfer curves and related transconductance g_m for the n-type conjugated polymer p(N-T) at increasing concentrations of d) polystyrene 10 KDa (PS10K) e) polystyrene 1 KDa (PS1K), and f) poly(methyl methacrylate) 10 KDa (PMM10K). All the measurements were acquired for drain voltage V_{DS} = 0.4 V with 0.1 M NaCl in water as the electrolyte. The gate was a silver pellet. The transfer curves are the average of a minimum of five devices. The measurements were acquired with a scan rate of 5.36 mV s^{-1}.

A significant drawback of p(N-T) is the rapid decline in device performance to 63% of the initial ON current after just 30 min of continuous ON/OFF cycling (at drain voltage (V_{DS}) of 0.4 V and gate voltage (V_G) ON/OFF cycles from 0 to 0.35 V), making it unsuitable for most applications such as sensors, where stable device operation is of essence to ensure reliable measurements.

To fabricate diluted OECTs, we blended p(N-T) with increasing amounts of insulating polymers, prepared by mixing stock solutions of 10 g L^{-1} p(N-T) with 50 g L^{-1} insulating polymer at different ratio in chloroform:o-dichlorobenzene (10:1 v/v, see Figure 1b and Table S1, Supporting Information). To study the impact of the "host" material on device performance, we chose three types of insulating polymer: polystyrene 10 kDa, polystyrene 1 kDa, and poly(methyl methacrylate) 10 KDa, hereafter referred to as PS10K, PS1K, and PMM10K, respectively. The two different types of PS are chosen to elucidate the impact of the molecular weight on the transport properties of the blend and device performance. Moreover, PMM allows the investigation of the influence of a more hydrophilic backbone – provided by the ester groups of PMM – on material and device properties.

We evaluated OECT performance using a silver pellet as the gate and 0.1 M NaCl in water as the electrolyte. As for devices made using the pristine p(N-T), all the diluted OECTs work in accumulation mode upon application of positive drain voltages V_{DS} and positive gate voltages V_G, consistent with the n-type character of p(N-T) and doping upon injection of Na^+ ions from the electrolyte solution (output characteristics can be found in Figure S1, Supporting Information and transfer characteristics in Figure 1d–f).

First, we investigated the impact of increasing amounts of insulator on the performance of diluted OECTs. OECT transfer characteristics of p(N-T):PS10K 1:3, with three styrene monomers for each monomer of p(N-T), does not lead to drastic changes in device current and transconductance (Figure 1d). Increasing the amount of PS10K to 6 styrene monomers for each monomer of p(N-T) leads to a drastic increase of maximum drain current and transconductance ($g_{m,max}$) from 0.16 mS for p(N-T) to 0.34 mS for p(N-T):PS10K 1:6. Increasing further the amount of PS10K to p(N-T):PS10K 1:17 leads to a decrease in $g_{m,max}$ to 0.12 mS, likely due to a disruption of the percolation network by high amounts of the insulator in the blend. Similar results were obtained for PS1K and PMM10K, where the monomer ratio p(N-T):insulator 1:6 exhibited the highest values of maximum transconductance. Thus, we focused on the p(N-T):insulator ratio 1:6 for further investigation.

Since the volume of the polymer in the channel is essential to compare different materials, we normalized maximum transconductance values to the area and thickness of the polymer films according to Equation 1. All the tested insulators showed that diluted OECTs with monomer ratio p(N-T):insulator 1:6 lead to an increase in OECT channel current and normalized transconductance $g_{m,norm}$ with respect to devices made with pristine p(N-T). If we compare the transfer characteristics for 1:6 p(N-T):insulator ratio across the three different insulators, we realize that PS10K leads to the highest $g_{m,norm}$ value of 2.0 mS cm^{-1}, followed by 1.0 mS cm^{-1} for PMM10K, and 0.9 mS cm^{-1} for PS1K (**Figure** 2a,b and **Table** 1). All the blends have a comparable threshold voltage of V_{TH} = 0.25 V with respect to pristine p(N-T), except for p(N-T):PS10K, exhibiting a V_{TH} of 0.27 V.

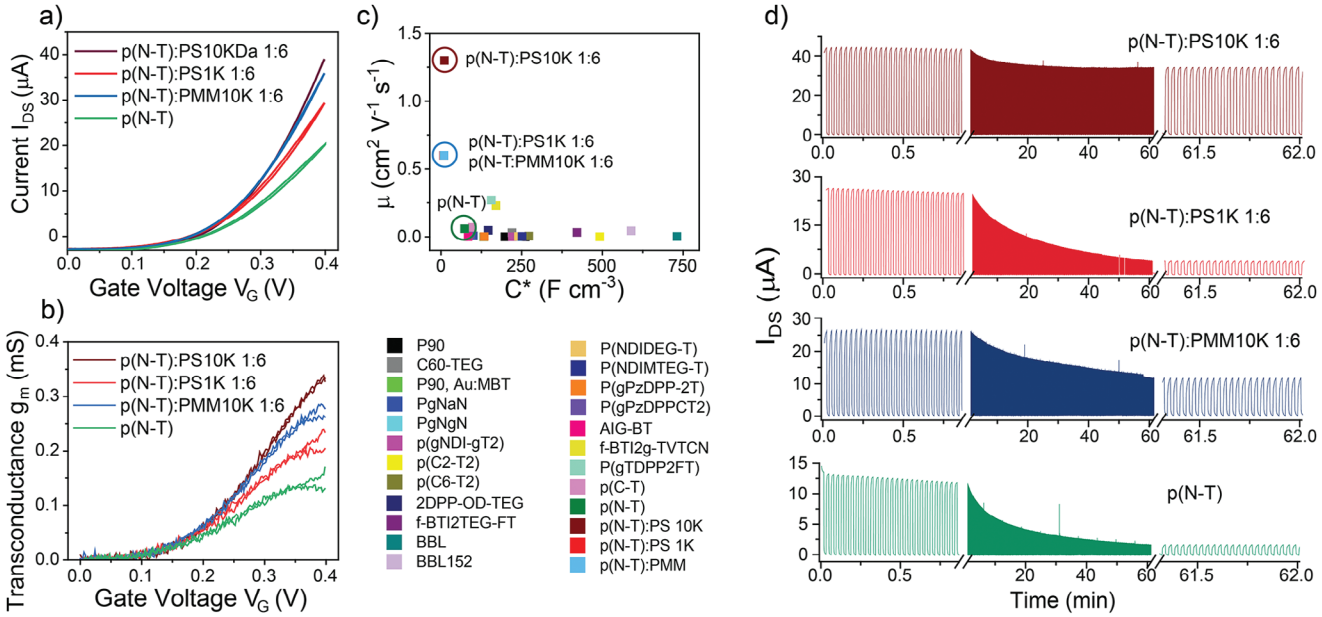

Figure 2. Averaged a) transfer characteristics and b) transconductance for p(N-T) (green), p(N-T): PS 10K (wine), p(N-T): PS 1K (red), and p(N-T):PMM 10K (blue) expressed in monomers of p(N:T) versus monomers of insulating polymer ratio. For all the measurements, V_{DS} = 0.4 V. The transfer curves are the average of a minimum of five devices. The measurements were acquired with an estimated scan rate of 5.36 mV s^{-1}. c) Mobility versus volumetric capacitance plot comparing the performance of p(N-T) and diluted p(N-T) (highlighted in a circle) with other channel materials for n-type OECTs reported in the literature (Table S2, Supporting Information). d) Representative stability for p(N-T) (green), p(N-T):PS10K 1:6 (wine), p(N-T):PS1K 1:6 (red), and p(N-T):PMM10K 1:6 (blue). For all the measurements, V_{DS} = 0.4 V and ON/OFF cycles were acquired at V_G ON/OFF steps from 0.4 to 0 V.

To evaluate blends performance, we calculated the product of electronic charge carrier mobility and volumetric capacitance μC* using the equation.

$$g_m = \mu C^* \cdot \frac{Wd}{L} \left| (V_{TH} - V_G) \right| \quad (1)$$

where W, d and L are the channel width, depth, and length, respectively, μ is the mobility, C* is the volumetric capacitance, V_{TH} is the threshold voltage, and V_G is the gate voltage. The μC* value for p(N-T):PS10K is 13.4 F V^{-1} cm^{-1} s^{-1}: an over threefold increase with respect to pristine p(N-T) with μC* = 4.3 F V^{-1} cm^{-1} s^{-1}. In contrast, PS1K and PMM10K show a modest increase in μC* of 5.3 and 4.9 F V^{-1} cm^{-1} s^{-1}, respectively.

We further used electrochemical impedance spectroscopy to extract the volumetric capacitances C* of the blends (see Figures S2–S5, Supporting Information and experimental section for details) and to understand the impact of the insulators on volumetric capacitance and electron mobility. As expected, the introduction of the insulators has a negative impact on the volumetric capacitance of the films, with a decrease of C* from 73 F cm^{-3} for p(N-T) to 10.1 F cm^{-3} for p(N-T):PS10K, 9.0 F cm^{-3} for p(N-T):PS1K, and 7.9 F cm^{-3} for p(N-T):PMM10K. We found however that the increase in transconductance and μC* for the blends is caused by a dramatic increase in the mobility of electron charge carriers from 0.059 cm^2 V^{-1} s^{-1} for p(N-T) to 0.6 cm^2 V^{-1} s^{-1} for p(N-T):PS1K, 0.6 cm^2 V^{-1} s^{-1} for p(N-T):PMM10K, and the record 1.3 cm^2 V^{-1} s^{-1} for p(N-T):PS10K. Comparison with other n-type OECT channel materials reported in the literature (Figure 2c and Table S2, Supporting Information) show that the blend p(N-T):PS10K 1:6 exhibits $\mu_{e,OECT}$ one order of magnitude higher than the best reported to date (0.27 cm^2 V^{-1} s^{-1} for P(gTDPP2FT)).

Our data agree well with previous reports showing increased charge carrier mobility upon diluting organic semiconductors

Table 1. Summary of OECT Parameters.

Polymer	$g_{m,norm}$ [a] [mS cm^{-1}]	V_{TH} [b] [v]	C* [d] [Fcm^{-3}]	μC* [e] [F V^{-1} cm^{-1} s^{-1}]	μ_{OECT} [c] [cm^2 V^{-1} s^{-1}]
p(N-T)	0.72 ± 0.23 [f]	0.25	73 ± 9 [f]	4.3 [f]	0.059 [f]
p(N-T):PS 10K 1:6	2.0 (1.6 ± 0.3)	0.27	10.1 ± 0.9	13.4 ± 2.8	1.3 ± 0.3
p(N-T):PMM 10K 1:6	1.0 (0.7 ± 0.2)	0.25	9.0 ± 0.5	5.3 ± 1.2	0.6 ± 0.1
p(N-T):PS 1K 1:6	0.9 (0.6 ± 0.2)	0.25	7.9 ± 1.0	4.9 ± 1.9	0.6 ± 0.2

[a] Maximum and average values calculated from different devices, transconductance normalized by the volume of the channel (W/Ld); [b] Values extrapolated by fitting the linear regime of the I_{DS}-V_{GS} plot; [c] Mobility values calculated from the μC* and the volumetric capacitance C*; [d] Volumetric capacitance values obtained by fitting the capacitance versus volume plot. Capacitance values are extracted from fitting the EIS curves; [e] values are extracted using Equation (1); [f] values previously reported.[24]

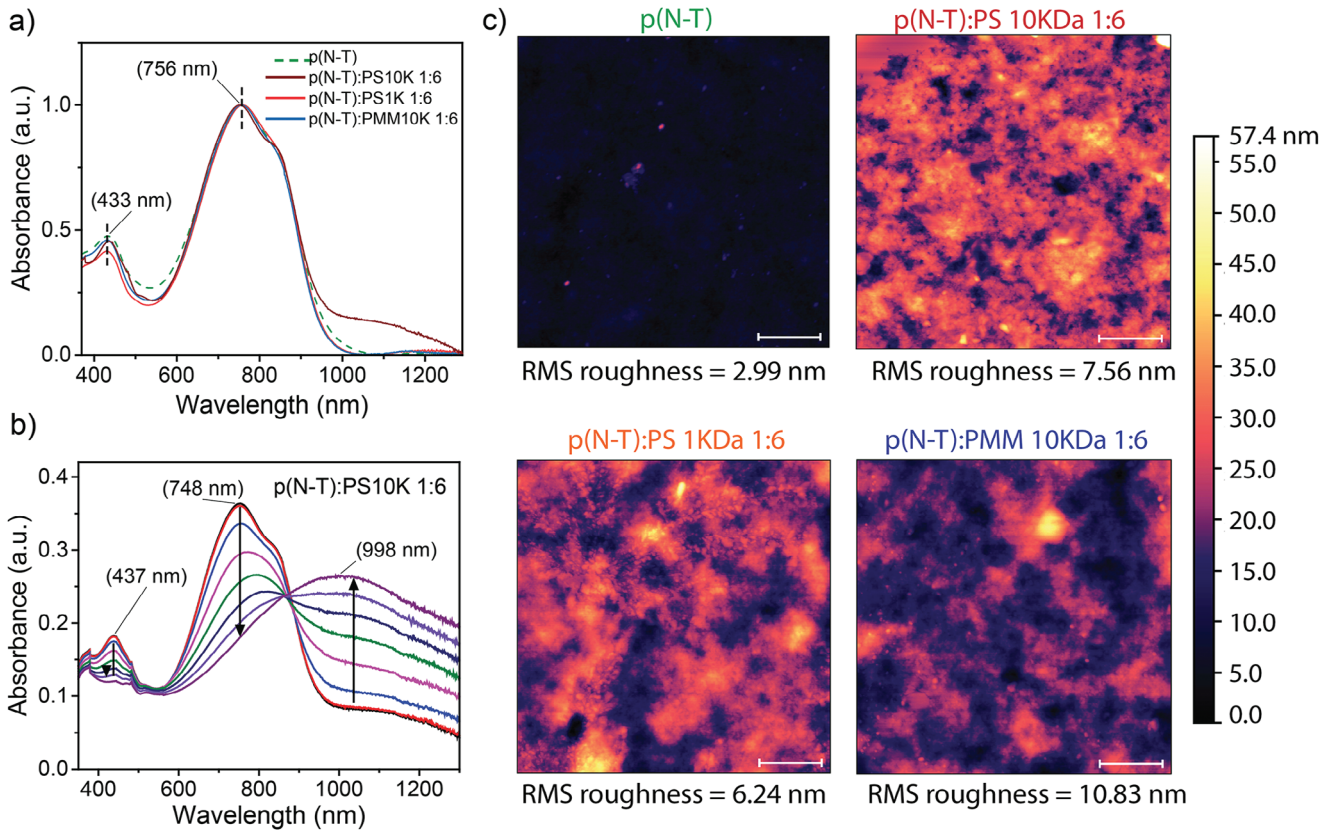

Figure 3. a) Normalized UV–vis-NIR absorption spectra of p(N-T) and p(N-T):insulators 1:6. b) UV–vis-NIR spectroelectrochemistry for p(N-T):PS10K 1:6. Data were acquired from 0 to −0.8 V with steps of 0.1 V. c) AFM data for p(N-T) and p(N-T):insulators. The scalebar is 1 µm.

with insulating polymers.[18,20,21] Similarly, as in field effect transistors, light-emitting diodes, and photovoltaics, we observe that this "dilution effect" is concentration dependent. For all the blends, device performance declines when the p(N-T):insulator ratio is increased to 1:17, likely due to an interruption in the interpenetrating network of semiconductor-rich phases.[21]

Stability is one of the most important criteria for OECT applications, particularly for sensors. Stability measurements at gate voltage steps from 0 to 0.4 V for p(N-T) show that devices retain only 12% of the original maximum drain current after over 60 min of ON/OFF switching (Figure 2d and Figure S6, Supporting Information). Blending with PS10K leads to a remarkable increase in device stability with respect to the pristine polymer, with p(N-T):PS10K 1:6 OECT retaining 77% of the initial maximum drain current $I_{D,max}$ after 1 hour of operation. A decline in current is visible in the first 10–15 minutes of operation, after which the maximum current settles at a constant value. Blending with PS1K didn't show the same effect, leading to a retention of just 15% of $I_{D,max}$ after 1 hour of operation. Blending with PMM 10K led to 44% of $I_{D,max}$ after over 1 hours of switching; an intermediate value between PS10K and PS1K. Overall, the data indicate that the molecular weight of the insulator and its hydrophobic/hydrophilic character impact not only the initial steady-state performance but also the operational stability upon ON/OFF switching.

To elucidate the impact of the insulators on the ion penetration within the polymer films, we acquired ON/OFF switching times. All devices show shorter OFF time constants with respect to the ON constants, in line with hydrated electrolyte ions penetration and release during the ON and OFF switches, respectively (Figure S7 and Table S3, Supporting Information). The ON time constant decreases in the order PS10K>PS1K>PMM10K, consistent with a slower penetration of hydrated electrolyte ions within the blends made using of the most hydrophobic polymers. In contrast, OFF processes were faster upon blending with PS1K with respect to the other two blends, which could be attributed to a larger extent of ion entrapment within the polymer network formed by the longer polymer chains.

To elucidate the effect of the insulators on the packing of the conjugated polymers in film form, we performed UV–vis-NIR absorption spectroscopy. All films show a high-energy band with a maximum at 433 nm, attributed to the π-π* transition, and another band with maximum absorption at 756 nm with a shoulder at ≈870 nm, ascribed to intermolecular charge transfer (ICT) (**Figure** 3a). In contrast to the other blends, p(N-T):PS10K exhibits a more pronounced vibrational shoulder, indicating a slightly stronger intrachain ordering in p(N-T) aggregates.[20] Moreover, another band appears at 1000–1200 nm, which might originate from strong intermolecular aggregation.[25]

UV–vis-NIR spectroelectrochemistry further shows that negative potentials from 0 to −0.8 V lead to a decrease in the π—π* and ICT bands, accompanied by the formation of a new absorption band in the NIR region (Figure 3b and Figure S8, Supporting Information) for p(N-T) and all the blends. The isosbestic point at

Table 2. Summary of GIWAXS Measurements.

Polymer		$q_{(100)}$ [Å^{-1}]	$d_{(100)}$ [Å]	$L_{c(100)}$ [Å]	$q_{(010)}$ [Å^{-1}]	$d_{(010)}$ [Å]	$L_{c(010)}$ [Å]	Dominant texture
p(N-T)	In-plane	0.27	23.26	40.26	1.80	3.49	46.40	Face-on
	Out-of-plane				1.80	3.49	31.71	
p(N-T):PS 10K 1:6	In-plane				1.82	3.45	53.63	Face-on
	Out-of-plane				1.82	3.45	42.64	
p(N-T):PS 1K 1:6	In-plane				1.81	3.47	47.80	Face-on
	Out-of-plane				1.81	3.47	36.42	
p(N-T):PMM 10K 1:6	In-plane				1.83	3.43	36.57	Face-on
	Out-of-plane				1.83	3.43	32.19	

≈880 nm marks the interconversion of p(N-T) to its reduced state. The absorption maximum of the new band, however, presents a red-shift from 956 nm for the pristine p(N-T) polymer, to 959 nm for p(N-T):PS1K, 965 nm for p(N-T):PMM10K, and 998 nm for p(N-T):PS10K. Such a shift could originate from changes in p(N-T) organization upon blending with different insulators.

We used atomic force microscopy (AFM) and Grazing-Incidence Wide-Angle X-ray Scattering (GIWAXS) to elucidate the impact of dilution on the microstructure of the films. AFM topography of p(N-T) shows a flat surface with root mean square (RMS) roughness of 2.99 nm (Figure 3c and Figure S9, Supporting Information). Blending of p(N-T) with insulating polymers (1:6 p(N-T):insulating polymer monomer ratio) results in the formation of aggregated domains, demonstrated by an increase in RMS roughness to 6.24 nm for p(N-T):PS1K, 7.56 nm for p(N-T):PS10K, and 10.83 nm for p(N-T):PMM10K. The data indicate that the domain size depends on the molecular weight and nature of the insulator, with a more extensive aggregation observed for PS1K, followed by PS10K, and PMM10K (Figure 3c). These features could originate from macro-phase separation in the polymer film, with the formation of insulator-rich and semiconductor-rich domains.[18,21] To confirm this hypothesis, we acquired AFM micrographs of the pristine insulating polymers (Figure S10, Supporting Information). The images show smooth features with RMS roughness of 4.59 nm PS1K, 1.35 nm for PS10K, and 1.17 nm for PMM10K, indicating that indeed the increase in the roughness and formation of aggregates results from the blending rather than aggregates already present in the pristine insulating polymers.

GIWAXS data show that both the pristine polymer and the blends have a face-on orientation (**Table 2** and Figures S11–S12, Supporting Information). The π—π stacking distance of p(N-T) is 3.49 Å in the in-plane and out-of-plane directions. Blending with insulating polymers leads to a slight decrease in (010) π—π diffraction peak both in the in-plane and out-of-plane directions to 3.47 Å for PS1K, 3.45 Å for PS10K, and 3.43 Å for PMM10K, indicating an undisturbed short-range intermolecular order upon p(N-T) dilution.

Among the insulators, we found that the insulator's type and molecular weight strongly impact the crystallite coherence length L_C. High molecular weight polystyrene (PS10K) leads to an increase in coherence length of the (010) peak both in-plane and out-of-plane, indicating larger crystalline domains in the p(N-T):PS10K films. Low molecular weight polystyrene (PS1K) leads to a similar trend to PS10K, with a modest increase in the coherence length of the (010) peak in-plane and out-of-plane. In contrast to PS10K and PS1K, blending with PMM10K leads to a decrease in the coherence length of (010) peak in-plane and a slight increase in the coherence length in the out-of-plane direction.

Previous studies of polymer blends have shown that the structure of both the conjugated and insulating polymer in terms of blend stoichiometry, choice of solvent, and molecular weight of the polymers have an impact on crystallization, phase separation, microstructure, thin film morphology, and charge carrier mobility of the films.[26]

Although PS and PMM are both amorphous polymers, there are main differences in their chemical structure that could cause a different interaction with p(N-T), leading to changes in the microstructure and morphology of polymer films. PS has phenyl groups in its chemical structure, while PMM has ester groups with electronegative (thus partially negatively charged) oxygen atoms. While PS can interact with p(N-T) via van-deer-Waals and π–π interactions (through its phenyl groups),[27] PMM can interact through a combination of electrostatic (both attractive and repulsive) and van-der-Waals forces. This can have a dramatic impact on the microstructure of a conjugated polymer with ethylene glycol side chains, like p(N-T), where polymer chains also interact via a combination of electrostatic (both attractive and repulsive) and van-der-Waals forces.[28]

The differences in the microstructure of the polymer films are also supported by AFM data, indicating that blending with PS (both 1 KDa and 10 KDa) results in a more extensive aggregation than blending with PMM 10 KDa.

Overall, AFM and GIWAXS data suggest that the observed increase in electronic mobility for the blends is linked to aggregation and modifications in the microstructure of the polymer films upon blending with the insulating polymers. The decrease in π-π stacking distance and the formation of large crystalline domains observed for p(N-T):PS10K 1:6 films correlate well with its superior charge transport among the blends.[29] In contrast, blending with the low molecular weight polystyrene PS1K leads to a minor decrease in π–stacking distance and increase in crystallite dimensions, which can be related to the smaller increases in charge carrier mobility with respect to PS10K. Blending with PMM10K leads to the shortest π-π stacking distance, but also a decrease in crystallite dimensions in the (010) peak in in-plane with respect to p(N-T), which could account for the comparable mobility with respect to p(N-T):PS1K 1:6.

As OECTs work in contact with aqueous solutions, we used contact angle measurements to elucidate the impact of the

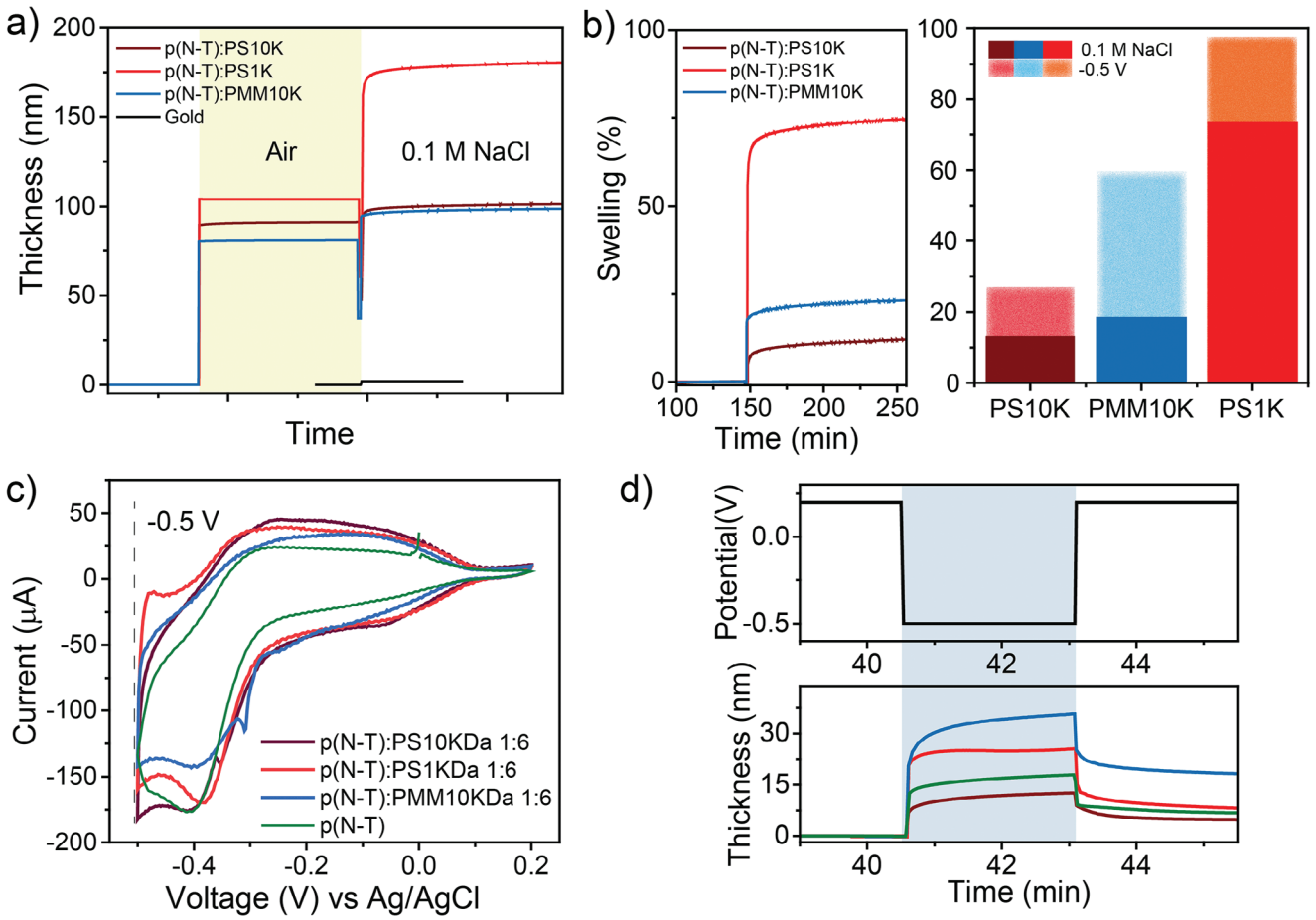

Figure 4. a) Stitched QCM-D data showing estimated changes in thickness after spin coating the polymer blends on top of the sensor and after flushing with 0.1 M $NaCl_{(aq)}$ at a constant rate of 0.1 mL min^{-1}. The black curve shows estimated changes in the recorded thickness of the bare Au sensor after changing the media from air to 0.1 M $NaCl_{(aq)}$. b) Swelling percentage of the films after exposure to 0.1 M $NaCl_{(aq)}$ with no applied bias and after application of −0.5 V versus Ag/AgCl. c) Cyclic voltammetry for the polymer films spin-coated on the sensors, acquired at a scan rate 0.1 V s^{-1}. d) Changes in thickness during chronoamperometry from open circuit voltage (V_{OC} = 0.2 V) to an applied bias of −0.5 V and vice versa.

insulating polymers on the wettability of the films. The data show an increase in contact angle from 102° for p(N-T) to 115° upon blending with both types of polystyrene (Figure S13 and Table S4, Supporting Information). In contrast, blending with PMM leads to a decrease in contact angle to 81°, due to the hydrophilic nature of ester groups. These data agree well with the ON switching times, showing slower penetration within the most hydrophobic films.

Electrochemical quartz crystal microbalance with dissipation monitoring (EQCM-D) data were then acquired to record in situ swelling of the films upon exposure to an aqueous electrolyte and injection of hydrated electrolyte ion from solution during electrochemical doping.[30]

First, we measured the QCM-D signals from the bare crystals in air (**Figures** 4a and S15, Supporting Information). Then, we removed the crystals and measured the signals for the polymer films in air. The films were then exposed to 0.1 M $NaCl_{(aq)}$ to monitor swelling upon exposure to the electrolyte.[31,32] Among the blends, p(N-T):PS1K shows the largest increase in film thickness from 104 to 180 nm, leading to 75% of passive swelling (Figure 4b and Table S5, Supporting Information). p(N-T):PMM10K films show a modest increase in the thickness from 83 to 98 nm (18% swelling), while p(N-T):PS10K undergoes the least changes from 87 to 98 nm (13% passive swelling). These data indicate that the molecular weight of the polymer has a strong impact on passive water and ion uptake from the electrolyte, with the largest changes observed for the short polystyrene.

Before EQCM-D measurements, we performed five break-in cycles using cycling voltammetry (CV) at potentials between 0.2 and −0.5 V versus Ag/AgCl. CV data show that all the films share a reduction peak at ≈−0.4 V, and an oxidation band at ≈−0.3 V (Figure 4c). Then, we acquired EQCM-D measurements using chronoamperometry by applying the oxidative potential of 0.2 V for 250 s, followed by reduction at −0.5 V for 250 s (Figure 4d and Figure S16, Supporting Information). Also in this case, p(N-T):PS10K undergoes the least changes, with 14% additional swelling. Blending with PS1K and PMM10K leads to a further 24% and 41% swelling, respectively. The additional swelling for p(N-T):PMM10K can be attributed to the higher polarity of PMM monomers that, in contrast to polystyrene, could help accommodate hydrated electrolyte ions through the formation of hydrogen bonds.[33] We note that the trend observed in swelling

percentage upon doping (PMM10K>PS1K> PS10K) does not correlate with the trend in C* PS10K≥PMM10K≥PS1K. A similar phenomenon was observed for polymers having a large extent of glycol side chains. In this case, the additional swelling was attributed to stabilizing water uptake, rather than increasing ion uptake, in the doped state.[32]

Overall, the data suggest that the hydrophobic nature of PS10K, combined with its high molecular weight, provides the lowest amounts of swelling upon electrochemical measurements, accounting for the higher stability of p(N-T) OECTs diluted with this insulating polymer. We note that, when the open circuit voltage of 0.2 V is applied again, the thickness of the p(N-T):PS10K does not fully return to the original value, indicating a non-reversible swelling of the polymer film upon application of reductive potentials and corroborating the initial decrease of I_{DS} current upon ON/OFF switching observed in stability measurements (Figure 2d).

The shorter chains of PS1K provide lower protection upon mass intake at the early stages of polymer contact with the electrolyte, which could account for the relatively poorer improvement in device stability upon p(N-T) dilution with PS1K. The hydrophilic nature of PMM10K causes the largest extent of swelling upon electrochemical measurements, which is likely to disrupt the polymer network during cycling, causing the observed irreversible changes in device performance.

To address whether this approach could be used with other n-type conjugated polymers, we blended p(C-T), p(C-2T), and f-BTI2g-TVTCN with polystyrene 10 KDa at a 1:6 monomer ratio.[24,9] p(C-T) is structurally similar to p(N-T), with the difference that isatins replace azaisatins groups within the acceptor unit. p(C-2T) has a similar chemical structure to p(C-T), with the difference that bis-thiophenes replace the thiophene donor units. In contrast, f-BTI2g-TVTCN has a completely different chemical structure, with fused bithiophene imide dimer (f-BTI2) as the acceptor unit and cyano-functionalized thienylene–vinylene–thienylene (TVT) as the donor unit. Our data show that, for all these polymers, blending with the hydrophobic PS10 KDa leads to an increase in the threshold voltage (Figures S17–S19, and Table S6, Supporting Information). The extent of the shift depends on the nature of the conjugated polymer, with the largest increase observed for f-BTI2g-TVTCN (from V_{TH} = 0.79 to 0.85 V). These data agree well with previous reports on the relation between the hydrophobicity of the polymer film and the threshold voltage. For OECTs operating in an aqueous electrolyte (e.g., 0.1 M $NaCl_{(aq)}$), increasing the hydrophobicity of the polymer film, for example, by replacing ethylene glycol side chains with alkyl side chains, results in an increase in threshold voltage.[34]

p(C-T) shows the largest increase in μC* from 3.4 to 8.9 F V^{-1} cm^{-1} s^{-1}. In contrast, no significant changes have been observed for p(C-2T), indicating that small changes in the chemical structure of the conjugated polymer have a large impact on blending dynamics and effective mixed ionic/electronic conductivity of the blend. f-BTI2g-TVTCN:PS 10K leads to a modest decrease in normalized transconductance ($g_{m,norm}$) from 23.68 to 19.72 S cm^{-1}, however, the sharper increase in transconductance (i.e., the steeper the slope of the curve) with respect to the pristine polymer determines an overall increase in μC* from 112.8 to 131.0 F V^{-1} cm^{-1} s^{-1}.

All the blends show an increase in operational stability with respect of the pristine polymers. Blending p(C-T) with PS10K leads to an increase of stability from 1.1% to 10.4% retain of the initial drain-source current after over 1 hour operation. P(C-2T) stability increases from 39.7% to 63.0% upon blending. f-BTI2g-TVTCN, the most stable polymer in the series (97.5% retain in initial drain current for the pristine polymer) leads to a further increase in drain current, reaching 129.5% of the original drain current after over 1 hour operation, which could be due to rearrangements in the polymer film upon switching.

Overall, the results indicate that several factors impact the mixed ionic/electronic conductivity and stability of n-type conjugated polymer:insulating polymer blends, such as the chemical structure of the conjugated and insulating polymers, the hydrophilic or hydrophobic character of the polymers, and the conjugated polymer:insulating polymer ratio.

3. Conclusions

The development of organic polymer blends such as PEDOT:PSS and BBL:PEI enabled conducting materials with major implications for various technologies, including the organic electrochemical transistor. The realization of n-type OECTs, having comparable performance with respect to p-type transistors, however, remains challenging.

Here, we demonstrated that blending n-type organic semiconductors with insulating commodity polymers can drastically improve the performance of organic electrochemical transistors while decreasing considerably the amount of conjugated polymer needed (six times less). We specifically showed that long polystyrene chains with 10 KDa molecular weight are the most effective in boosting OECT performance for the semiconducting polymer p(N-T), leading to enhanced polymer mobility by two orders of magnitude. This drastic increase compensates for the loss in volumetric capacitance caused by the addition of the insulating polymer, leading to an overall increase in μC* by over three times with respect to the pristine conjugated polymer. Data on the microstructure of the films show that these changes are due to an increase in the packing of the conjugated polymer chains, leading to better charge transport. In addition, the diluted polymer blend displays a considerable increase in device stability from 12% retain of the initial maximum drain current for p(N-T) to 77% for p(N-T):PS10K 1:6. EQCM-D measurements showed that such an increase in stability is related to a decrease in swelling of the films both upon hydration and electrochemical doping.

We showed that this method can be applied also to improve the OECT performance of other types of n-type conjugated polymer. However, the mixed ionic/electronic transport of the blend and device stability is influenced by several parameters, such as the chemical structure and hydrophilic character of the polymers and their blending ratio. Future work will focus on providing a deeper understanding on the physical parameters underlying blend dynamics and to determine if this approach could be extended further to other materials including p-type conjugated polymers.

Our work shows that blending an n-type conjugated polymer with insulating polymers enables to develop organic mixed ionic/electronic conductors with the highest electronic mobility reported so far for n-type OECTs (1.3 cm^2 V^{-1} s^{-1}). For diluted organic semiconductors, it has been demonstrated that such an

increase in mobility originates from the suppression of charge carrier trapping sites upon dilution.[18] Better methods to quantify charge carrier traps in organic mixed ionic/electronic conductors (OMIECs) in OECT configuration would be needed to verify if this is the case also for diluted OMIECs. Overall, dilution of OMIECs with cheap insulating polymers paves the way for affordable high-performance n-type organic iontronics.

4. Experimental Section

Materials: All the chemicals were ordered from Sigma-Aldrich and stored according to the vendor's instructions unless otherwise stated. The polymer p(N-T), (3E,7E)−3-(6-methyl-1-(2,5,8,11,14,17-hexaoxanonadecan-19-yl)−2-oxo-1,2-dihydro-3H-pyrrolo[2,3-b]pyridin-3-ylidene)−7-(6-(5-methylthiophen-2-yl)−1-(2,5,8,11,14,17-hexaoxanonadecan-19-yl)−2-oxo-1,2-dihydro-3H-pyrrolo[2,3-b]pyridin-3-ylidene)−3,7-dihydrobenzo[1,2-b:4,5-b −′]difuran-2,6-dione, was synthesized as previously described.[24] The chosen insulating polymers were polystyrene Mw ≈10 000 g mol^{-1}, polystyrene Mw ≈1110 g mol^{-1}, and poly(methyl methacrylate) Mw ≈10 900 g mol^{-1}. Stock solutions were prepared with concentration of 10 mg mL^{-1} for p(N-T) and 50 mg mL^{-1} for the insulating polymers in chloroform:o-dichlorobenzene 10:1 v/v with 5 vol% bromoanisole. Blends were prepared having a final concentration of 6 mg mL^{-1} for p(N-T) and a p(N-T):insulating polymers ratio of 1:0, 1:6, and 1:17 in monomer weight. For more details, see Table S1, Supporting Information.

UV–vis-NIR Absorption Spectroscopy: UV–vis-NIR absorption spectra were acquired with a PerkinElmer Lambda 950 UV–vis-NIR spectrophotometer. Thin films of the polymer blends were prepared by spin-coating their solutions onto Indium Tin Oxide (ITO)-coated glass substrates. Prior to spin-coating, the ITO glasses were cleaned by ultrasonication in soapy water for 15 min, followed by basic piranha cleaning in a solution of H_2O:H_2O_2:NH_3 at ≈70 °C for 5–10 min, and then dried using an air gun.

Cyclic Voltammetry: CV measurements were performed using a Metrohm Autolab/PGSTAT101 potentiostat. The three-electrode setup consisted of an Ag/AgCl (3 M KCl aqueous solution) as the reference electrode, a Pt wire as the counter electrode, and thin films of the polymer spin-coated on ITO-coated glass substrates as the working electrode. Films of the polymers were prepared as described for UV–vis-NIR absorption measurements. 0.1 M NaCl in water was used as the electrolyte.

UV–vis-NIR Spectroelectrochemistry: Spectroelectrochemical measurements were performed with a similar setup as for CV measurements, with the three-electrode setup fitted inside a quartz cuvette. Amperometric measurements were carried out by applying subsequent potentials with steps of 0.1 V. The potentials were applied for 15 s prior to recording each absorption spectrum to ensure complete film stabilization at that potential. An aqueous 0.1 M NaCl solution was used as the supporting electrolyte.

Atomic Force Microscopy: AFM measurements were carried out using the tapping mode of Bruker Dimension Icon AFM with a XSC11/PT silicon tip from MikroMasch (cantilever T = 270 nm, L = 210 µm, W = 30 µm, f0 = 80 kHz, k = 2.7 N m^{-1}). All polymer films were prepared by spin-coating at 1000 rpm for 60 s and annealing in the oven at 120 °C for 10 min. A 5 × 5 µm area was imaged at 5 different locations on the spin-coated polymer on the glass substrate with a resolution of 512 × 512 pixels. All the AFM images were processed using the Gwyddion 2.56 software, and the statistical parameters, including the roughness, were calculated using the "Statistical Parameter" tool on Gwyddion.

Grazing-incidence Wide-angle X-ray Scattering: Samples for GIWAX were prepared as described for Uv–vis-NIR absorption measurements, with the only difference that p+ doped silicon wafers were used as the substrates. The wafers were cleaned by subsequential sonication steps in soapy water, ethanol, and isopropanol for 15 min each. An incidence angle of 0.18° and a photon energy of 8 keV were used to record the scattering patterns.

Fabrication of Organic Electrochemical Transistors: Electrode contacts were prepared by lift-off process. Thermal evaporation was used to deposit 10 nm of chromium or titanium as an adhesion layer and 50 nm of gold on soda-lime glass. Each channel had length L = 20 µm and width W = 500 µm. Solutions of the polymer blends were spin-coated at 1000 rpm for 60 s and annealed in the oven at 120 °C for 10 min. Film thicknesses were measured with by a Tencor profilometer. The obtained film thicknesses were 85.5 ± 3.7 nm for p(N-T):PS10K, 150.2 ± 3.1 nm for p(N-T):PS1K, and 164.9 ± 30.8 nm for p(N-T):PMM10K. 0.1 M NaCl in water was used as the electrolyte and a silver pellet as the gate. Device characterization was performed in air at room temperature using a Keithley 4200A-SCS parameter analyzer (Tektronix, USA) equipped with two source measurement units (SMU) and one pulse measurement unit (PMU). The PMU was used to measure the ON and OFF OECT switching times, which were calculated as the time it took to reach 90% or 10% of the maximum drain current, respectively. The switching times were acquired for OECTs having channels with dimensions 10 × 100 µm (LxW).

Electrochemical Impedance Spectroscopy: EIS measurements were performed using a BioLogic VSP potentiostat. The polymers were spin-coated on top of square gold electrodes with an active area 4 or 8 mm^2 at spin speed of either 1000 rpm or 4000 rpm for 60 sec followed by annealing in the oven at 120 °C. The polymer films on gold were used as the working electrode, an Ag/AgCl (3 M KCl aqueous solution) as the reference electrode, and a platinum coil as a counter electrode. The electrolyte was an aqueous 0.1 M NaCl solution. EIS measurements were performed at −0.4 V. The frequency was scanned from 100 kHz to 10 Hz at a sinus amplitude of 10 mV. The capacitance was extracted by fitting the data to a modified Randle's circuit model Rs(Rp||Q),[25] where Rs is the electrolyte resistance, Q is a constant phase element, and Rp is the charge transfer resistance, using ZFit (EC-Lab V11.41 software). The thickness of the films was determined in a dry state with a Tencor profilometer.

Contact Angle Measurements: Contact angle measurements were performed using a ThetaLite optical tensiometer (TL100, Biolin Scientific). The contact angle was measured on at least three different areas on each sample by dropping a 20 µL drop of deionized water and recording a video (not shown). The video frames were then analyzed using the OneAttension software to calculate the average contact angle for each sample.

Electrochemical Quartz Crystal Microbalance with Dissipation Monitoring: QCM-D measurements were performed using a Q-sense analyzer (QE 401, Biolin Scientific, Gothenburg, Sweden). First, gold-coated QSense sensors (QSX 301) were measured in air and after introducing 0.1 M NaCl in milli-Q water at a constant rate of 0.1 mL min^{-1}. This allowed us to assess the shifts in the QCM-D signals due to changes in media density from air to the aqueous electrolyte. For polymer film analysis, the crystals were unloaded from the measuring chambers and used as substrates for spin-coating of the polymer films. The polymers were spin-coated at 2500 rpm for 60 s and annealed in the oven at 120 °C for 10 min. The crystals were placed back in the chamber and QCM-D signals were acquired again in air. After frequency *f* and dissipation *d* signals stabilized (i.e., Δf < 1 Hz/2 min), we flushed in a solution of 0.1 M NaCl in milli-Q water at a constant rate of 0.1 mL min^{-1}. After the measurements, we used the QSoft software function "stitch data" to combine the measurements of the bare crystals with those of the spin-coated polymer films. The data were then modeled using the Sauerbrey equation within the QSense Dfind software (Biolin Scientific). The model assumed the use of a gold crystal in air as the initial reference, followed by the addition of a polymer layer of density comparable to polystyrene (1.0 g cm^{-3}) in air, and flushing with an aqueous electrolyte solution with density of 1.04 g cm^{-3}.

EQCM-D measurements were performed with a QSense electrochemistry module (QEM 401) connected to a Metrohm Autolab/PGSTAT101 potentiostat. The module was equipped with a Pt counter electrode, an Ag/AgCl reference electrode, and the polymer-coated gold sensor as the working electrode. 0.1 M NaCl in milli-Q water was the electrolyte. After film hydration, we waited again for the signal to be flat before starting with the electrochemical measurements. First, a cyclic voltammetry was performed at potentials between 0.2 and −0.5 V at a scan rate of 0.1 V s^{-1}.

Then, we performed a chronoamperometric measurement by stepping the potential from 0.2 V (fully undoped) to −0.5 V (fully doped) and 0.2 V again for 150 s each.

Swelling was calculated as the percentage change in thickness relative to the dry thickness (T_{dry}), assuming that all the films had the same surface area determined by the area of the gold sensor (0.7854 cm^2)

$$Swelling\ \% = \frac{T_{total} - T_{dry}}{T_{dry}} * 100 \quad (2)$$

Supporting Information

Supporting Information is available from the Wiley Online Library or from the author.

Acknowledgements

E.Z. and A.H. gratefully acknowledge the Knut and Alice Wallenberg Foundation (Grant No. KAW2015.0178, 2020.0206, 2021.0312), and the Swedish Research Council (Grant No. 2018–03483, 2022-04060, and International Postdoc Grant No. 2017–06381). E.Z. gratefully acknowledges the Göran Gustafsson Foundation, the Swedish Research Council (Grant No. 2022-02855), and Formas – a Swedish Research Council for Sustainable Development (Grant No. 2022-00374) for support. This project has received funding from the European Union's Horizon 2020 research and innovation program under the Marie Sklodowska-Curie grant agreement No 101025599. W.Y. and Y.W. thank the National Natural Science Foundation of China (Grant No. 22275212 and 21875291),National Key R&D Program (Grant No. 2022YFA1206600) and Fundamental Research Funds for the Central Universities-Sun Yat-sen University (Grant No. 23yxqntd002). This work was supported by AIMES – The center for integrated medical and engineering sciences (www.aimes.se), Karolinska Institutet (1-249/2019), KTH Royal Institute of Technology (VF-2019-0110), and Getinge AB (4.1599/2018). This work was partially supported by Digital Futures and by the Wallenberg Initiative Materials Science for Sustainability (WISE) funded by the Knut and Alice Wallenberg Foundation. X.G. is grateful to the financial support by the Guangdong Provincial Key Laboratory Program (Grant No. 2021B1212040001). This work was partially supported by European Union's Horizon 2020 Framework Programme H2020-WIDESPREAD-01-2016-2017-TeamingPhase2 under grant agreement No.739508, project CAMART2.

Conflict of Interest

The authors declare no conflict of interest.

Data Availability Statement

The data that support the findings of this study are available from the corresponding author upon reasonable request.

Keywords

conjugated polymer, diluted organic semiconductors, organic bioelectronics, organic electrochemical transistor, organic mixed ionic-electronic conductor

Received: March 21, 2023
Revised: February 8, 2024
Published online: March 10, 2024

[1] S. Ting, M. Tan, A. Gumyusenge, T. J. Quill, G. Swain Lecroy, G. E. Bonacchini, I. Denti, A. Salleo, *Adv. Mater.* **2022**, *34*, 2110406.
[2] B. D. Paulsen, K. Tybrandt, E. Stavrinidou, J. Rivnay, *Nat. Mater.* **2019**, *19*, 13.
[3] G. Malliaras, I. McCulloch, *Chem. Rev.* **2022**, *122*, 4323.
[4] E. Zeglio, O. Inganäs, *Adv. Mater.* **2018**, *30*, 1800941.
[5] J. Rivnay, S. Inal, A. Salleo, R. M. Owens, M. Berggren, G. G. Malliaras, *Nat. Rev. Mater.* **2018**, *3*, 17086.
[6] M. Moser, J. F. Ponder, A. Wadsworth, A. Giovannitti, I. McCulloch, *Adv. Funct. Mater.* **2019**, *29*, 1807033.
[7] S. Yu, C. J. Kousseff, C. B. Nielsen, *Synth. Met.* **2023**, *293*, 117295.
[8] K. Feng, W. Shan, S. Ma, Z. Wu, J. Chen, H. Guo, B. Liu, J. Wang, B. Li, H. Y. Woo, S. Fabiano, W. Huang, X. Guo, *Angew. Chem., Int. Ed.* **2021**, *60*, 24198.
[9] K. Feng, W. Shan, J. Wang, J.-W. Lee, W. Yang, W. Wu, Y. Wang, B. J. Kim, X. Guo, H. Guo, *Adv. Mater.* **2022**, *34*, 2201340.
[10] A. Giovannitti, I. P. Maria, D. Hanifi, M. J. Donahue, D. Bryant, K. J. Barth, B. E. Makdah, A. Savva, D. Moia, M. Zetek, P. R. F. Barnes, O. G. Reid, S. Inal, G. Rumbles, G. G. Malliaras, J. Nelson, J. Rivnay, I. McCulloch, *Chem. Mater.* **2018**, *30*, 2945.
[11] D. Ohayon, A. Savva, W. Du, B. D. Paulsen, I. Uguz, R. S. Ashraf, J. Rivnay, I. McCulloch, S. Inal, *ACS Appl. Mater. Interfaces* **2021**, *13*, 4253.
[12] C. Y. Yang, M. A. Stoeckel, T. P. Ruoko, H. Y. Wu, X. Liu, N. B. Kolhe, Z. Wu, Y. Puttisong, C. Musumeci, M. Massetti, H. Sun, K. Xu, D. Tu, W. M. Chen, H. Y. Woo, M. Fahlman, S. A. Jenekhe, M. Berggren, S. Fabiano, *Nat. Commun.* **2021**, *12*, 2354.
[13] A. F. Paterson, A. Savva, S. Wustoni, L. Tsetseris, B. D. Paulsen, H. Faber, A. H. Emwas, X. Chen, G. Nikiforidis, T. C. Hidalgo, M. Moser, I. P. Maria, J. Rivnay, I. McCulloch, T. D. Anthopoulos, S. Inal, *Nat. Commun.* **2020**, *11*, 3004.
[14] A. Savva, D. Ohayon, J. Surgailis, A. F. Paterson, T. C. Hidalgo, X. Chen, I. P. Maria, B. D. Paulsen, A. J. Petty II, J. Rivnay, I. McCulloch, S. Inal, *Adv. Electron. Mater.* **2019**, *5*, 1900249.
[15] A. Elschner, S. Kirchmeyer, W. Lövenich, U. Merker, K. Reuter, *PEDOT: Principles and Applications of an Intrinsically Conductive Polymer*, CRC Press, Boca Raton **2010**.
[16] H. J. Kim, K. Perera, Z. Liang, B. Bowen, J. Mei, B. W. Boudouris, *ACS Macro Lett.* **2022**, *11*, 243.
[17] X. Strakosas, M. Sessolo, A. Hama, J. Rivnay, E. Stavrinidou, G. G. Malliaras, R. M. Owens, *J. Mater. Chem. B* **2014**, *2*, 2537.
[18] D. Abbaszadeh, A. Kunz, G. A. H. Wetzelaer, J. J. Michels, N. I. Crăciun, K. Koynov, I. Lieberwirth, P. W. M. Blom, *Nat. Mater.* **2016**, *15*, 628.
[19] A. Kunz, P. W. M. Blom, J. J. Michels, *J. Mater. Chem. C* **2017**, *5*, 3042.
[20] B. Tan, H. Pan, H. Li, M. L. Minus, B. M. Budhlall, M. J. Sobkowicz, *J. Phys. Chem. C* **2018**, *122*, 2918.
[21] C. Wang, X. Liu, Y. Xiao, J. Bergqvist, X. Lu, F. Gao, M. Fahlman, *Sol. RRL* **2020**, *4*, 2000261.
[22] J. Rivnay, *Nat. Mater.* **2016**, *15*, 594.
[23] S. Goffri, C. Müller, N. Stingelin-Stutzmann, D. W. Breiby, C. P. Radano, J. W. Andreasen, R. Thompson, R. A. J. Janssen, M. M. Nielsen, P. Smith, H. Sirringhaus, *Nat. Mater.* **2006**, *5*, 950.
[24] Y. Wang, E. Zeglio, L. Wang, S. Cong, G. Zhu, H. Liao, J. Duan, Y. Zhou, Z. Li, D. Mawad, A. Herland, W. Yue, I. McCulloch, *Adv. Funct. Mater.* **2022**, *32*, 2111439.
[25] W. Zhang, Z. Mao, Z. Chen, J. Huang, C. Wei, D. Gao, Z. Lin, H. Li, L. Wang, G. Yu, *Polym. Chem.* **2017**, *8*, 879.
[26] Z. He, Z. Zhang, S. Bi, *Mater. Adv.* **2022**, *3*, 1953.
[27] W. Cai, D. Xu, L. Qian, J. Wei, C. Xiao, L. Qian, Z. Y. Lu, S. Cui, *J. Am. Chem. Soc.* **2019**, *141*, 9500.
[28] S. Moro, N. Siemons, O. Drury, D. A. Warr, T. A. Moriarty, L. M. A. Perdigão, D. Pearce, M. Moser, R. K. Hallani, J. Parker, I. McCulloch, J. M. Frost, J. Nelson, G. Costantini, *ACS Nano* **2022**, *16*, 21303.

[29] B. Meng, H. Song, X. Chen, Z. Xie, J. Liu, L. Wang, *Macromolecules.* **2015**, *48*, 4357.
[30] A. Savva, R. Hallani, C. Cendra, J. Surgailis, T. C. Hidalgo, S. Wustoni, R. Sheelamanthula, X. Chen, M. Kirkus, A. Giovannitti, A. Salleo, I. McCulloch, S. Inal, *Adv. Funct. Mater.* **2020**, *30*, 1907657.
[31] L. Q. Flagg, C. G. Bischak, J. W. Onorato, R. B. Rashid, C. K. Luscombe, D. S. Ginger, *J. Am. Chem. Soc.* **2019**, *141*, 4345.
[32] M. Moser, T. C. Hidalgo, J. Surgailis, J. Gladisch, S. Ghosh, R. Sheelamanthula, Q. Thiburce, A. Giovannitti, A. Salleo, N. Gasparini, A. Wadsworth, I. Zozoulenko, M. Berggren, E. Stavrinidou, S. Inal, I. McCulloch, *Adv. Mater.* **2020**, *32*, 2002748.
[33] D. Li, J. Brisson, *Polymer* **1998**, *39*, 793.
[34] A. Giovannitti, D.-T. Sbircea, S. Inal, C. B. Nielsen, E. Bandiello, D. A. Hanifi, M. Sessolo, G. G. Malliaras, I. McCulloch, J. Rivnay, *Proc. Natl. Acad. Sci. U. S. A.* **2016**, *113*, 12017.
[35] C. G. Bischak, L. Q. Flagg, K. Yan, C. Z. Li, D. S. Ginger, *ACS Appl. Mater. Int.* **2019**, *11*, 28138.
[36] A. F. Paterson, H. Faber, A. Savva, G. Nikiforidis, M. Gedda, T. C. Hidalgo, X. Chen, I. McCulloch, T. D. Anthopoulos, S. Inal, *Adv. Mater.* **2019**, *31*, 1902291.
[37] J. Surgailis, A. Savva, V. Druet, B. D. Paulsen, R. Wu, A. Hamidi-Sakr, D. Ohayon, G. Nikiforidis, X. Chen, I. McCulloch, J. Rivnay, S. Inal, *Adv. Funct. Mater.* **2021**, *31*, 2010165.
[38] X. Chen, A. Marks, B. D. Paulsen, R. Wu, R. B. Rashid, H. Chen, M. Alsufyani, J. Rivnay, I. McCulloch, *Angew. Chem.* **2021**, *133*, 9454.
[39] I. P. Maria, B. D. Paulsen, A. Savva, D. Ohayon, R. Wu, R. Hallani, A. Basu, W. Du, T. D. Anthopoulos, S. Inal, J. Rivnay, I. McCulloch, A. Giovannitti, *Adv. Funct. Mater.* **2021**, *31*, 2008718.
[40] J. J. Samuel, A. Garudapalli, A. A. Mohapatra, C. Gangadharappa, S. Patil, N. Phani, B. Aetukuri, *Adv. Funct. Mater.* **2021**, *31*, 2102903.
[41] H. Y. Wu, C. Y. Yang, Q. Li, N. B. Kolhe, X. Strakosas, M. A. Stoeckel, Z. Wu, W. Jin, M. Savvakis, R. Kroon, D. Tu, H. Y. Woo, M. Berggren, S. A. Jenekhe, S. Fabiano, *Adv. Mater.* **2022**, *34*, 2106235.
[42] D. Jeong, I.-Y. Jo, S. Lee, J. H. Kim, Y. Kim, D. Kim, J. R. Reynolds, M.-H. Yoon, B. J. Kim, *Adv. Funct. Mater.* **2022**, *32*, 2111950.
[43] J. Shi, P. Li, X. Y. Deng, J. Xu, Z. Huang, Y. Lei, Y. Wang, J. Y. Wang, X. Gu, T. Lei, *Chem. Mater.* **2022**, *34*, 864.
[44] Z. S. Parr, J. Borges-González, R. B. Rashid, K. J. Thorley, D. Meli, B. D. Paulsen, J. Strzalka, J. Rivnay, C. B. Nielsen, *Adv. Mater.* **2022**, *34*, 2107829.
[45] P. Li, J. Shi, Y. Lei, Z. Huang, T. Lei, *Nat. Commun.* **2022**, *13*, 5970.
[46] Y. Wang, E. Zeglio, H. Liao, J. Xu, F. Liu, Z. Li, I. P. Maria, D. Mawad, A. Herland, I. Mcculloch, W. Yue, *Chem. Mater.* **2019**, *31*, 9797.
[47] J. Chen, S. Cong, L. Wang, Y. Wang, L. Lan, C. Chen, Y. Zhou, Z. Li, I. McCulloch, W. Yue, *Mater Horiz.* **2023**, *10*, 607.